Fault diagnosis model of the variable torque pumping unit well based on the power-displacement diagram

Fault diagnosis model of the variable torque pumping unit well based on the power-displacement diagram

Dechun Chen[1], Ruiqi Zhou[1, *], Hongxia Meng[1], Yuandong Peng[2], Feng Chang[3], Dong Jiang[3], Bin Wei[3]

[1]China University of Petroleum, Qingdao, Shandong, 266580, China
[2]SINOPEC Henan Oilfield Branch, Zhengzhou, Henan, 473000, China
[3]SINOPEC Shengli Oilfield Branch, Dongying, Shandong, 257000, China

*Corresponding author e-mail: RichyChou33@163.com

Abstract. This work proposes a new method of diagnosing the variable torque pumping unit well, by analysing the eigenvalue of power-displacement diagram. Considering the actual angular velocity, the unbalanced weight of structure and the efficiency of motor and gearbox, the relationship between the polished rod load and the input power of motor are derived by analysing the internal relation between the polished rod load, the output shaft torque of the gearbox, the output shaft power of motor and the input power of motor. Then, the conversion model of the power-displacement diagram based on the dynamometer card is derived. By transforming the dynamometer card in typical working condition into the corresponding power-displacement diagram, 11 power-displacement diagrams in typical working conditions are established. By extracting the grayscale statistical eigenvalues from typical power-displacement diagrams, a working condition diagnosis model of oil well is established based on the grey correlation analysis. The test of 5 wells in the oilfield shows the average relative error of average normalized power of up and down stroke between the measured power-displacement diagram and the calculated power-displacement diagram are 6.31% and 5.83%, and the average fitting coefficient is 0.91. This shows that this model has a good accuracy, and it also proves the reliability of the typical power-displacement diagram. According to the test of 80 wells in the oilfield, the accuracy of diagnosis results based on the measured power-displacement diagram is 93.3%. This shows that the model has high accuracy and practicability, and can provide technical support for intelligent diagnosis and production optimization decision in production system of variable torque pumping unit well.

1. Introduction

The variable torque pumping unit has been widely used in oilfield [1]. The failure analysis of variable torque pumping unit well based on the dynamometer card is the main method of current production fault analysis. The diagnosis process can be divided into feature extraction from dynamometer card and diagnosing based on model [2]. In the field of feature extraction, Wang [3] and Zhong [4] analyzed dynamometer card by mapping the curve into a gray matrix for gray scale analysis. Han [5] and Li [6] represent the dynamometer card with Freeman chain code, and extracted feature to construct a

designated mode set. Liu et al. [7] extracted feature from dynamometer card by autoencoder, and used features as inputs to the classification algorithms. Reges Jr et al. [8] proposes a new method of diagnosis by analyzing segments between the points of opening and closing valves identified in the dynamometer cards. As for diagnosis model, some research efforts have been reported through stochastic models, e.g., support vector machine (SVM) [9, 10, 11] and artificial neural network (ANN) [12, 13, 14], etc.

The power-displacement diagram is used to diagnose the working conditions of pumping unit by using the closed curve of the motor input power and displacement of the suspension center. Compared with the dynamometer card, the power-displacement diagram can not only reflect the condition of downhole equipment, but also diagnose the condition of surface equipment [15, 16]. However, due to the lack of typical power-displacement diagrams of variable torque pumping unit, it's difficult to realize the failure analysis of oil well based on the power-displacement diagram, so the data cannot be used effectively. Therefore, we deduced a power-displacement diagram conversion model based on the dynamometer card, established 11 typical power-displacement diagrams of variable torque pumping unit well, built fault diagnosis model based on typical power-displacement diagrams. This provides theoretical basis and technical support for the real-time intelligent diagnosis and production optimization decision of the variable torque pumping unit well.

2. The conversion model of dynamometer card and power-displacement diagram

2.1. Output shaft torque calculation model of gearbox

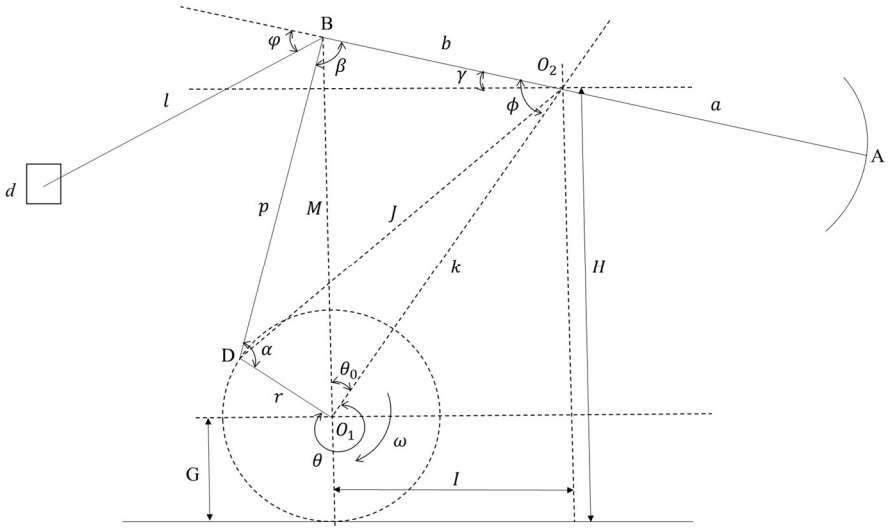

Figure 1. The geometric schematic diagram of the variable torque pumping unit.

The geometric schematic diagram of the variable torque pumping unit is shown in Figure 1. The torque balance equation of crank output shaft is

$$Tr + W_t r \sin\theta = F_p r \sin\alpha \tag{1}$$

Then

$$T = F_p \sin\alpha - W_t \sin\theta \tag{2}$$

Considering the unbalanced weight of structure of the pumping unit and the influence of the counterweight, the moment balance analysis of the saddle bearing is

$$\left(P_A - B\right)a = \pm F_p^{'} b\sin\beta + m_{Wd}a_{Wd}l_a + W_d l_{Wd} \tag{3}$$

Then

$$F_p^{'} = \pm\frac{\left(P_A - B\right)a - m_{Wd}a_{Wd}l_a - W_d l_{Wd}}{b\sin\beta} \tag{4}$$

The sign of the first term on the right side of the equation is plus in the upstroke, and minus in the downstroke, the same below.

F_p And $F_p^{'}$ are equal and in the opposite direction. So the output shaft torque of gearbox is

$$M = Tr = F_p r\sin\alpha - W_t r\sin\theta = \pm\frac{\left(P_A - B\right)a - m_{Wd}a_{Wd}l_a - W_d l_{Wd}}{b\sin\beta}\cdot r\sin\alpha - W_t r\sin\theta \tag{5}$$

2.2. The relationship between polished rod load and motor power.

The relationship between the motor input power and the output shaft torque of gearbox is [17]

$$M = \frac{9549N_d\eta_t}{n} \tag{6}$$

Combine formula (5) and formula (6), the calculation model for the motor input power according to the polished rod load is

$$N_d = \frac{n}{9549\eta_t}[\pm\frac{\left(P_A - B\right)a - m_{Wd}a_{Wd}l_a - W_d l_{Wd}}{b\sin\beta}\cdot r\sin\alpha - W_t r\sin\theta] \tag{7}$$

2.3. Steps for calculating the power-displacement diagram based on the dynamometer card

(1) The displacement and load of the suspension point in one stroke can obtained by dynamometer installed on the pumping unit.

(2) According to the displacement of the suspension point, the ϕ can be calculated as

$$\phi = \phi_{\max} - \frac{180S_i}{a\pi} \tag{8}$$

(3) α And β can be calculated from ϕ as

$$\alpha = \arccos\left(\frac{p^2 + r^2 - E^2}{2pr}\right) \tag{9}$$

$$E = \sqrt{b^2 + k^2 - 2bk\cos\phi} \tag{10}$$

When it's in upstroke, β can be calculated as

$$\beta=\arccos\left(\frac{b^2+E^2-k^2}{2bE}\right)-\arccos\left(\frac{p^2+E^2-r^2}{2pE}\right) \tag{11}$$

When it's in downstroke, β can be calculated as

$$\beta=\arccos\left(\frac{b^2+E^2-k^2}{2bE}\right)+\arccos\left(\frac{p^2+E^2-r^2}{2pE}\right) \tag{12}$$

(4) According to the α, β and θ, a_{Wb} can be calculated as

$$a_{Wd}=-a_A\frac{l_a}{a} \tag{13}$$

$$a_A=\frac{-a\omega^2 rk}{b^2 p}\frac{r\sin\alpha\cos\beta\sin\theta_k+b\sin\beta\cos\alpha\sin\phi}{\sin^3\beta} \tag{14}$$

$$l_a=\sqrt{b^2+l^2-2bl\cos(180-\varphi)} \tag{15}$$

$$\theta_k=\theta-\theta_0 \tag{16}$$

(5) From the above calculated parameters and known parameters, the motor input power can be calculated through equation 7, where

$$W_t=\frac{W_c R_c}{r} \tag{17}$$

$$\gamma=\frac{\pi}{2}-\theta_0-\arccos\left(\frac{k^2+b^2-E^2}{2Kb}\right) \tag{18}$$

$$l_{Wd}=l\cos(\varphi+\gamma)+b\cos\gamma \tag{19}$$

(6) Draw the relation curve between motor input power and displacement of suspension point, and get the power-displacement diagram.

3. Analysis of the power-displacement diagram in typical working conditions

3.1. Normalization processing of the power-displacement diagram

$$N_{gy(i)}=(N_{(i)}-N_{\min})/(N_{\max}-N_{\min}) \tag{20}$$

$$x_{gy(i)}=(x_{(i)}-x_{\min})/(x_{\max}-x_{\min}) \tag{21}$$

3.2. Power-displacement diagrams in typical working conditions

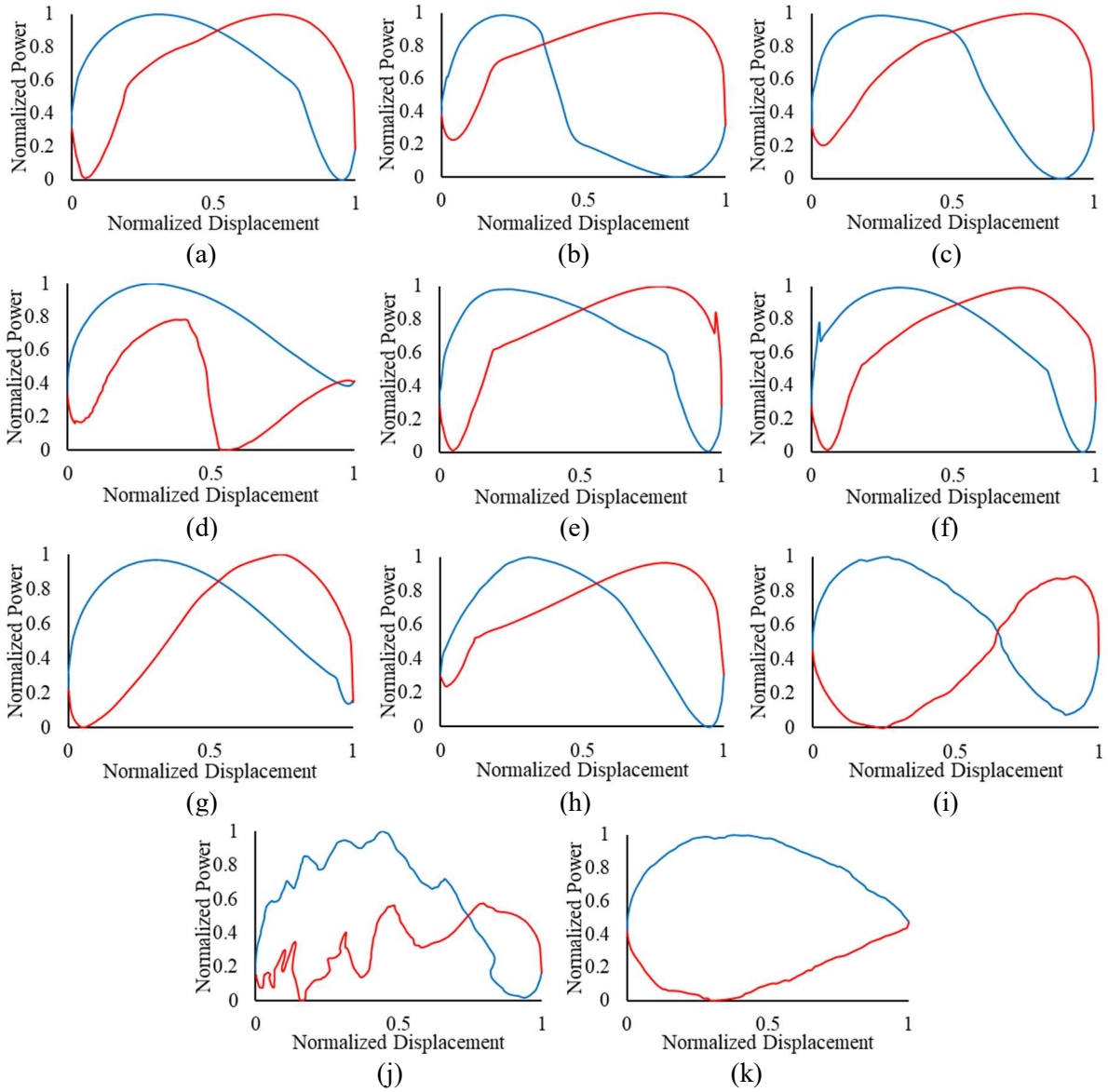

Figure 2. Normalized power-displacement diagram in typical working conditions

11 theoretical dynamometer cards in typical working conditions are selected and converted into power-displacement diagrams. The normalized power-displacement diagram of well in normal is shown in Figure 2(a). The power peak of the up and down stroke are basically the same with the pumping unit in equilibrium, and the variation trend of curve is basically the same. At the end of the upstroke loading curve and downstroke unloading curve, the curve has obvious inflection points. The slope of curve is larger in the loading segment and the unloading segment, and is smaller in the load stable segment. The displacement of the intersection point of curve is near 0.5.

The normalized power-displacement diagram of well with insufficient fluid supply is shown in Figure 2(b). The variation trend of the upstroke curve is basically the same as the curve of normal working condition. Due to the untimely unloading of the polished rod load, the power value of the starting segment of curve is low and the change is small, and it only rises rapidly after the unloading begins. There are two inflection points on the downstroke curve at the starting point and ending point of

unloading. Compared with the normal working condition, the displacement of the inflection point is move to the left.

The normalized power-displacement diagram of well with gasinfluence is shown in Figure 2(c). Due to the slow opening of the standing valve in the upstroke, the load line of the dynamometer card is change gently, and the corresponding power curve has no obvious inflection point at the end of loading. Because the traveling valve open slowly, the unloading becomes slower in the downstoke, and the displacement of the inflection point is move to the left compared with the normal working condition.

The normalized power-displacement diagram of well with pump plunger out of the pump barrel is shown in Figure 2(d). Because the pump plunger is out of the pump barrel in the upstroke, the polished rod is suddenly unloaded, and curve drops rapidly and then slowly increases until the upstroke ends. There are two obvious inflection points on the upstroke curve. The downstroke curve has no inflection point because the downstroke has no unloading process. The power peak of upstroke is obviously lower than the power peak of downstroke.

The normalized power-displacement diagram of well with pump plunger hits the top of pump barrel is shown in Figure 2(e). The pump plunger hits the pump barrel at the top dead center, resulting in a sudden increase in load, and the upstroke curve has a prominent bulge near the top dead center.

The normalized power-displacement diagram of well with pump plunger hits the bottom of pump barrel is shown in Figure 2(f). The pump plunger hits the pump barrel at the bottom dead center, resulting in a sudden decrease in load, and the downstroke curve has a prominent bulge near the bottom dead center.

The normalized power-displacement diagram of well with traveling valve leaking off is shown in Figure 2(g). At the beginning of the upstroke, the load changes gently because the polished rod load cannot be loaded in time, and there is no inflection point on the upstroke curve. Due to the early unloading of the polished rod load in the upstroke, the unloading line of the dynamometer card becomes shorter, so the displacement of the inflection point is move to the right compared with the normal working condition.

The normalized power-displacement diagram of well with standing valve leaking off is shown in Figure 2(h). At the beginning of the upstroke, due to the preloading of the polished rod load at the end of the last stroke, the load line of the dynamometer card is shortened, so the displacement of the inflection point is move to the left compared with the normal working condition. At the beginning of the downstroke, the curve has no obvious inflection point because the slowly unloading of the polished rod.

The normalized power-displacement diagram of well with stuck pump is shown in Figure 2(i). The curve is in the form of "∞", and approximately vertical symmetry about the straight with a normalized power value of 0.5. The stuck point of the pump plunger is corresponding to the intersection point of curve. The counterbalancing of the pumping unit is determined by the position of the stuck point. If the stuck point is close to the top dead point, the pumping unit is in overbalance. If the stuck point is close to the bottom dead point, the pumping unit is in unbalanced.

The normalized power-displacement diagram of sand well is shown in Figure 2(j). There are many prominent bulges on the curve.

The normalized power-displacement diagram of well with rod parting is shown in Figure 2(k). The curve is approximately vertical symmetry about the straight with a normalized power value of 0.5. The normalized power value of upstroke is constant less than 0.5, and the normalized power value of downstroke is constant greater than 0.5.

3.3. Fault diagnosis model

The normalized power-displacement diagram is placed in a 100×100 grid, and the grid values are initialized to 0. The gray value of the grids passing by the curve are assigned as 1, and then the gray level matrix can be calculated [4]. According to the principle of mathematical statistics, six grayscale statistical eigenvalues can be calculated by gray level matrix, which are used as the eigenvalue in fault

diagnosis. The grayscale statistical eigenvalue include gray mean, gray variance, gray skewness, gray kurtosis, gray energy and gray entropy [18].

Table 1. Grayscale statistical eigenvalues of typical power-displacement diagrams.

	Mean	Variance	Skewness	Kurtosis	Energy	Entropy
Normal	1.831	5.456	6.112	5.536	3.905	0.0102
Insufficient fluid supply	1.691	5.511	6.759	6.169	3.937	0.0099
Gasinfluence	1.860	5.552	7.041	6.545	3.922	0.0100
Standing valve leaking off	2.064	5.672	6.852	6.293	3.996	0.0093
Traveling valve leaking off	1.972	5.541	5.328	4.760	3.931	0.0099
Pump plunger hits the top of pump barrel	1.883	5.426	6.724	6.122	3.898	0.0103
Pump plunger hits the bottom of pump barrel	1.977	5.455	5.709	5.133	3.918	0.0101
Pump plunger out of the pump barrel	1.527	5.248	5.839	5.076	3.845	0.0108
Stuck pump	1.640	5.155	6.308	5.337	3.836	0.0109
Rod parting	2.068	5.749	5.756	4.966	4.146	0.0080
Sand well	1.116	5.187	4.552	3.848	3.736	0.0121

The grayscale statistical eigenvalues of the power-displacement diagram in 11 typical working conditions were calculated, as shown in Table 1. After calculating the eigenvalue of the diagnosed power-displacement diagram, the calculated eigenvalue and the eigenvalue in table 1 should be analyzed by grey correlation analysis, and the working condition of oil well can be inferred according to the maximum grey correlation degree.

4. Application analysis

4.1. The calculation and analysis of the power-displacement diagram conversion model

Based on Visual Basic language, we established calculation and analysis models of power-displacement diagram, and compiled software for analysis. Input the structural parameters and other known data of the pumping unit into the software, and import the measured dynamometer card and the measured power-displacement diagram data. These data are usually the displacement of 200 test points within one stroke, as well as the corresponding load and power values, which can obtained by dynamometer installed on the pumping unit. The calculated power-displacement diagram and analysis results can be obtained by software calculation.

Taking X01 well as example for calculation and analysis. The measured diagram are shown in the Table 2.

Table 2. The measured diagram of X1 well

Measured dynamometer card	Measured power-displacement diagram
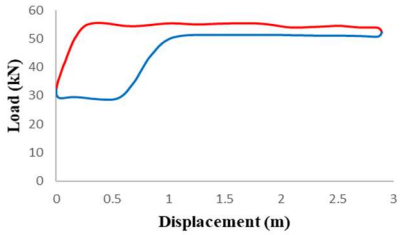	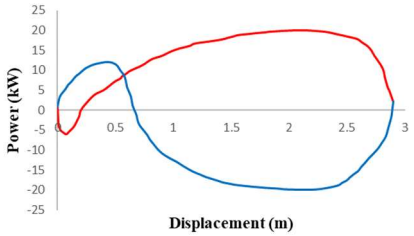

The calculated power-displacement diagram (dashed line) is compared with the measured power-displacement diagram (solid line) after normalization, which is shown in Figure 3.

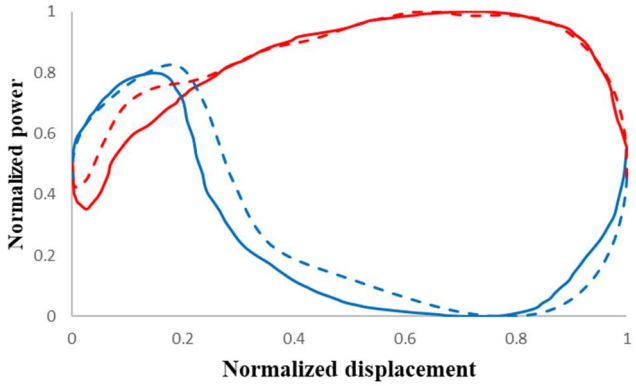

Figure 3. Comparison of power-displacement diagram

Comparing the calculated power-displacement diagram with the measured power-displacement diagram, the variation trend and characteristics of curve are consistent, and the fitting degree of curve is high.

The relative error of the average normalized power of upstroke is

$$E_{r(\text{umax})} = \left| \frac{N_{u\,\max(\text{calculated})} - N_{u\,\max(\text{measured})}}{N_{u\,\max(\text{measured})}} \right| = \left| \frac{0.80 - 0.75}{0.75} \right| = 6.67\%$$

The relative error of the average normalized power of downstroke is

$$E_{r(d\,\max)} = \left| \frac{N_{d\,\max(\text{calculated})} - N_{d\,\max(\text{measured})}}{N_{d\,\max(\text{measured})}} \right| = \left| \frac{0.31 - 0.34}{0.34} \right| = 8.82\%$$

The fitting coefficient of the curve is

$$R^2 = \frac{S_h^2}{S_h^2 + S_c^2} = \frac{10.75}{10.75 + 0.95} = 0.92$$

The closer R^2 is to 1, the better the curve fitting effect is.

The result of conversion calculation of power-displacement diagram of 5 wells are shown in Table 3. The average relative error of average normalized power of up and down strokes of the measured power-displacement diagram and the calculated power-displacement diagram of 5 wells are 6.31% and 3.83% respectively, and the average fitting coefficient is 0.91. This shows that the conversion model has good accuracy, which proves the reliability of typical power-displacement diagram and its eigenvalues.

Table 3. The comparison between measured and calculated power-displacement diagram

Well No.	Relative error of the average normalized power of upstroke	Relative error of the average normalized power of downstroke	Fitting coefficient
X2	6.67%	8.82%	0.92
X8	8.67%	2.66%	0.91
X10	1.24%	1.75%	0.97
X25	7.57%	3.69%	0.89
X33	7.39%	2.22%	0.84

4.2. Diagnosis and analysis of oil well based on power-displacement diagram

Taking X1 well as example, the actual working condition of this well is insufficient fluid supply. The grayscale statistical eigenvalue of the measured power-displacement diagram were calculated and used as the reference sequence for gray correlation analysis with compare sequences composed of the eigenvalues in Table 1. Grey correlation degrees are (0.83, 0.90, 0.88, 0.78, 0.71, 0.87, 0.72, 0.88, 0.70, 0.66, 0.68). According to the maximum grey correlation degree of 0.90, the working condition diagnosis result of X1 well is insufficient fluid supply.

Based on the measured power-displacement diagram, the diagnosis result of 80 wells are shown in Table 4.

Table 4. Coincidence rate of diagnosis results

Actual working condition	Well number	Coincidence rate of diagnosis results
Normal	18	94.4%
Insufficient fluid supply	12	91.7%
Gasinfluence	10	90%
Standing valve leaking off	12	91.7%
Traveling valve leaking off	10	90%
Stuck pump	10	90%
Pump plunger out of the pump	8	100%
Total	80	93.3%

5. Conclusions

The conversion model of the power-displacement diagram based on the dynamometer card is derived based on the analysis of the actual angular velocity, the unbalanced weight of the structure and the efficiency of motor and gearbox. According to the calculation test of 5 wells, the average relative error of average normalized power of up and down strokes of the measured power-displacement diagram and the calculated power-displacement diagram is 6.31% and 3.83% respectively, and the average fitting coefficient is 0.91. This shows that the model has high accuracy and proves the reliability of the typical power-displacement diagram based on this model.

The power-displacement diagram of 11 typical working conditions is established and used as the basis for fault diagnosis model of variable torque pumping unit well based on measured power-displacement diagram. According to the test of 80 wells, the coincidence rate between diagnosis result and actual working condition is 93.3%. This shows that the model has high accuracy and practicability.

6. Nomenclature

T = the shear force of crank pin, kN
r = the crank radius, m
Wt = the weight of crank converted to the crank radius, kN
θ = the angle between the crank and vertical upward direction along clockwise, °
Fp = the force of the pitman on the crank, kN
α = the angle between the crank and pitman, °
PA = the polished rod load, kN
B = the unbalanced weight of structure, kN
a = the distance between A and O2, m
F'p = the force of crank on the pitman, kN
b = the distance between B and O2, m
β= the angle between b and pitman, °
mWd = the mass of the counterweight, kg
aWd = the acceleration of the center of gravity of the counterweight, m/s2
la = the distance between the fulcrum and the counterweight, m
Wd = the weight of the counterweight, kN

lWd = the distance between the point of the gravity center of the counterweight projected on the horizontal line and the fulcrum, m

M = the output shaft torque of gearbox, kN·m

Nd = the motor input power, kW

n = the pumping speed, r/min

ηt = the total transmission efficiency from the motor to the gearbox output shaft (including motor efficiency, belt efficiency and gearbox efficiency), dimensionless

ϕ = the angle between b and k, °

Si =the displacement of point i, m

p= the length of pitman, m

aA=the acceleration of the polished rod, m/s2

ω = the angular velocity of the crank, rad/s

φ = the angle between l and the extension line of b, m

θ0 =the angle between E and k, °

Wc = the weight of the crank, kN

Rc = the radius of the center of gravity of the crank, m

γ =the angle between b and the horizontal line, °

Ngy(i) = the normalized power of the point i, dimensionless

xgy(i) = the normalized displacement of the point i, dimensionless

Nmax = the maximum power of the power-displacement diagram, kW

Nmin = the minimum power of the power-displacement diagram, kW

N(i) = the measured power of the point i, kW

xmax = the maximum displacement of the power-displacement diagram, m

xmin = the minimum displacement of the power-displacement diagram, m

x(i) = the measured displacement of the point i, m

Sh2 = the regression sum of squares, dimensionless

Sc2 = the residual sum of squares, dimensionless

Acknowledgments

We would like to thank SINOPEC henan oilfield branch for providing data and funding for this research project. We would also like to thank other collaborators whose work has indirectly helped in this project.

References

[1] Tang Jingfei, Wu Xiaodong, Ma Guorui, Gao Zhaomin. 2011. Calculation of Suspension Point Load on Adjustable Diameter Pumping Unit. Oil Field Equipment 40(11):37-40. doi: 10.3969/j.issn.1001-3482.2011.11.010.

[2] Liu Fu, Liu Qingyou, Wang Hailan. 2003. Operating Performance's Simulation of A New Energy-saving Controllable Diameter and Variable Torque Pumping Unit. Drilling & Production Technology (01):68-70+4-5. doi: 10.3969/j.issn.1006-768X.2003.01.023.

[3] Wang X, Guan C, Gao R. 2014. The improved grey correlation fault diagnosis for oil pumping well. Paper presented at the International Conference on Measurement, Information and Control. IEEE. doi: 10.1109/MIC.2013.6758170.

[4] G.X. Zhong, M.M. Zou. 2016. Exploring failure characteristics of indicator diagram of reciprocating pump based on gray matrix. Mechanical Science & Technology for Aerospace Engineering 35 (2) 279–284. doi:10.13433/j.cnki.1003-8728.2016.0221.

[5] Han Ying, Li Kun. 2016. Integrated fault diagnosis method for down-hole working conditions of the beam pumping unit. Paper presented at the Control & Decision Conference. IEEE. doi: 10.1109/CCDC.2016.7532248.

[6] Li Kun, Gao Xianwen, Yang Weibing, et al. 2013. Multiple fault diagnosis of down-hole conditions of sucker-rod pumping wells based on Freeman chain code and DCA. Petroleum Science 10(3):347-360.

[7] Jeremy Liu, Ayush Jaiswal, Ke-Thia Yao, Cauligi S. Raghavendra. 2015. Autoencoder-derived Features as Inputs to Classification Algorithms for Predicting Well Failures. Society of Petroleum Engineers. doi:10.2118/174015-MS.
[8] Galdir D. Reges Jr., Leizer Schnitman, Ricardo Reis, Fabricio Mota. 2015. A New Approach to Diagnosis of Sucker Rod Pump Systems by Analyzing Segments of Downhole Dynamometer Cards. Society of Petroleum Engineers. doi:10.2118/173964-MS.
[9] Kun Li, Xianwen Gao, Zhongda Tian, et al. 2013. Using the curve moment and the PSO-SVM method to diagnose downhole conditions of a sucker rod pumping unit. Petroleum Science 10(1):73–80. doi:10.1007/s12182-013-0252-y.
[10] Wei Wu, Yu Zhou, Hangxin Wei. 2013. A fault diagnosis of sucker rod pumping system based on SVM. Applied Mechanics and Materials 307:285–289. doi: 10.4028/ www. scientific. net/ AMM. 307.285.
[11] Feng J, Wang M, Yang Y, et al. 2012. Fault Diagnosis of Sucker-Rod Pumping System Using Support Vector Machine. Communications and Information Processing. Springer Berlin Heidelberg. doi:10.1007/978-3-642-31968-6_22.
[12] Peng Xu, Shijin Xu, Hongwei Yin. 2007. Application of self-organizing competitive neural network in fault diagnosis of sucker rod pumping system. Journal of Petroleum Science & Engineering 58(1):43-48. doi:10.1016/j.petrol.2006.11.008.
[13] Nazi G M, Ashenayi K, Lea J F, et al. 1994. Application of Artificial Neural Network to Pump Card Diagnosis. Society of Petroleum Engineers 6(6):9-14. doi:10.2118/25420-PA.
[14] Wu ZhengJia, Huang ShaoXiong, Luo YueSheng. 2013. Research on Automatic Diagnosis Based on ANN Well Conditions Fault. doi:10.2991/isca-13.2013.6.
[15] Chen Dechun, Xiao Liangfei, Zhang Ruichao, et al. 2017. A Diagnosis Model on Working Condition of Pumping Unit in Oil Wells Based on Electrical Diagrams. Journal of China University of Petroleum(Edition of Natural Science) 41(2):108-115.
[16] Chen Dechun, Lv Fei, Yao Ya, et al. 2017. A New Model Based on the Electrical Diagrams for Diagnosing the Working Status of Belt-Pump-Uint Wells. Petroleum Geology & Oilfield Development in Daqing 36(05):119-123. doi:10.19597/J.ISSN.1000-3754.201610026.
[17] Li Hujun, Zhang Jifen, Zhi Lianyou. 1991. Predicting Dynamometer Cards by Actual Motor Power Curves. Petroleum Geology & Oilfield Development in Daqing (04):63-67+34. doi:10.19597/j.issn.1000-3754.1991.04.009.
[18] Wu Wei, Chen Guoding, He Yan. 2007. Fault diagnosis system for pump work indicating diagram based on neural network and gray-level matrix[J]. Journal of Xi'an Shiyou University(Natural Science Edition) 22(3):119-121. doi:10.3969/j.issn.1673-064X.2007.03.029.